RSC Advances

PAPER

View Article Online
View Journal | View Issue

Cite this: *RSC Adv.*, 2015, **5**, 6462

Efficient improvement of photoelectrochemical activity for multiple semiconductor (CdS/PbS/ZnS) co-sensitized TiO_2 photoelectrodes by hydrogen treatment

Dong Ding,[a] Yanli Chen,[a] Pin Lv,[a] Huizhen Yao,[a] Yannan Mu,[ab] Shi Su,[a] Xiaolin Zhang,[a] Liying Zhou,[a] Wuyou Fu[a] and Haibin Yang*[a]

Received 16th October 2014
Accepted 15th December 2014

DOI: 10.1039/c4ra12491j

www.rsc.org/advances

In the present work we report a simple and viable approach to improve the photoelectrochemical activity of TiO_2 photoelectrodes. Firstly, a TiO_2 nanotube array film with nanowires directly formed on top (denoted as TiO_2NTWs) was prepared by a simple electrochemical anodization method on a titanium foil. Then the pristine TiO_2NTWs were annealed in a hydrogen atmosphere (denoted as H*TiO_2NTWs). Subsequently, the formation of a CdS, PbS, and ZnS quantum dot (QD) sensitized H*TiO_2NTW photoelectrode was carried out by successive ionic layer adsorption and reaction (SILAR). The best performance of the photoelectrode was TiO_2 NTWs annealed in hydrogen at 350 °C with 4 cycles of CdS plus 2 cycles of PbS and 3 cycles of ZnS. A maximum short-circuit photocurrent density of 3.62 mA cm^{-2} was obtained under an illumination of AM 1.5 G, which can boost the photocurrent density of the pristine TiO_2NTWs by up to 503%. The enhancement was attributed to the extension of the light absorption range by hydrogen treatment and QD sensitization.

1. Introduction

Titanium dioxide (TiO_2) is a semiconductor most widely used in dye solar cells, highly efficient photocatalysts and ultrasensitive biosensors.[1] One-dimensional nanostructured TiO_2 such as TiO_2 nanoparticles, TiO_2 nanowires and TiO_2 nanotubes, are widely used as semiconductor photoelectrodes for a variety of solar-driven clean energy and environmental technologies.[2,3] However, TiO_2 nanoparticles structure has trap sites that cause charge recombination at the contact interface between TiO_2 nanoparticles. To overcome this disadvantage, studies of nanostructured TiO_2 photoelectrodes like TiO_2 nanotubes, that offer a direct path of electrons, have been carried out.[4] In this study, TiO_2 nanotubes with nanowires directly formed on top (denoted as TiO_2NTWs) was prepared by electrochemical anodization on a titanium foil. Since there is no grain boundary between the tubes and the wires, the TiO_2NTWs structure would inherit the advantages of both the nanotube and nanowire in charge separation, electronic transport, and light harvesting.[5–7] Thus, it shows higher change collection efficiency than other TiO_2 nanometer materials.

As we all known, the effectiveness of photoactive processes underlying water decontamination, hydrogen production and solar cell is dictated to a great extent by the semiconductor's ability to absorb UV and visible-light, as well as its capability of restraining the rapid combination of photo-generated electrons and holes.[4,8,9] However, the photoelectrochemical properties of TiO_2 is substantially limited by its large band gap energy ($E_g \approx$ 3.2 eV) and this limits its absorption to the ultraviolet region which takes only about 3–5% of the solar spectrum. There have been persistent efforts to vary the band gap of TiO_2 by doping metal or nonmetal impurities that generate donor or acceptor states in the band gap.[10–12] But almost every method to dope metal or nonmetal impurities into TiO_2 was complicated and limited in commercial application. It is equally important to improve the electronic structure of TiO_2 for effective separation and transportation of photoexcited charge carriers. Yat Li *et al.* used hydrogen treatment (annealed TiO_2 nanowires in hydrogen) as a simple and effective strategy to fundamentally improve the performance of TiO_2 nanowires for photoelectrochemical (PEC) water splitting.[13] It was reported that oxygen vacancies play a critical role in determining the electronic properties of TiO_2 [13–18] and annealing TiO_2 nanostructures in a reducing gas atmosphere such as hydrogen will increase the density of oxygen vacancies (donor density). The formation of oxygen vacancies could shallow donor states below conduction band originating from Ti 3d orbitals, which can even overlap the conduction band in the case of highly deficient TiO_2. The increase of the concentration of electrons enhances the electrical conductivity of TiO_2,[19–23] and thereby improves the

[a]State Key Laboratory of Superhard Materials, Jilin University, Changchun 130012, PR China. E-mail: yanghb@jlu.edu.cn; Fax: +86 431 85168763; Tel: +86 431 85168763
[b]Department of Physics and Chemistry, Heihe University, Heihe 164300, PR China

photoelectrochemical performance. Meanwhile vast amount of researches have been focused on enhancing the visible light absorption of TiO_2 such as sensitization with small band gap semiconductors, *e.g.*, CdS,[24–27] CdTe,[5] CdSe,[28] SnS_2,[29] PbS.[30,31] Lin *et al.* used a simple sequence chemical bath deposition technique to prepare stable and uniform nanostructured TiO_2/CdS/ZnS photoelectrode in an alcohol solution system.[32] Lee *et al.* have shown that multilayered semiconductor (CdS/CdSe/ZnS) layers prepared by SILAR on the surface of TiO_2 mesoporous films.[33] And this versatile approach improves the efficiency of light usage by modifying optical absorption coefficient and wavelength of TiO_2 photoelectrodes. Although studies focusing on the sensitization of TiO_2 with PbS, CdS has been widely investigated, there are few reports about the combination effect of hydrogen treatment and PbS and CdS quantum dots (QDs) co-sensitization for these highly ordered, self-assembled TiO_2NTWs for photoelectrochemical application.

Herein, the photoelectrochemical activity of TiO_2NTWs was dramatically enhanced through a simple method named H-SILAR. First, the as-prepared TiO_2NTWs were annealed in hydrogen (denoted as H*TiO_2NTWs). Second, we modified H*TiO_2NTWs by SILAR technique. In this paper, CdS and PbS have been used as sensitizers since their narrow band gap 2.25 eV and 1.30 eV, respectively, which means CdS and PbS can trigger wider light absorption range compared to TiO_2.[34] We have investigated the effect of hydrogen processing on the photoelectrochemical performance of TiO_2NTWs, and explored the optimum condition of quantum dots sensitization. Our result shows that the H*TiO_2/CdS/PbS/ZnS heterostructured exhibit substantially higher visible-light-driven photoactivity with maximum short-circuit photocurrent density of 3.62 mA cm^{-2}. The capability of making highly photoactive H*TiO_2/CdS/PbS/ZnS heterostructured opens up new opportunities in various areas, including PEC water splitting, dye-sensitized solar cells, *etc.* A detailed synthesis process, characterization, and photoactivity of this sample are discussed in this paper.

2. Experimental section

2.1 Preparation of self-assembled TiO_2NTWs

All chemicals used were of the highest purity available and used as received without further purification. Deionized water (18 MΩ cm) was used in all cases. TiO_2NTWs were prepared by electrochemical anodization of a titanium foil (4 cm × 3 cm, 0.4 mm thick, 99.9% purity). Titanium foil was cleaned by sonication in acetone, isopropanol and ethanol, and followed by rinsing with deionized water and drying in flow of nitrogen before anodization. Titanium foil was used as an anode, with a graphite plate as cathode in an ethylene glycol electrolyte solution containing 0.3 wt% NH_4F and 5.0 vol% deionized H_2O. Electrochemical anodizaiton was carried out on a direct current (dc) stabilized voltage and current power supply (WYJ60V3A, Pingguo instrumentation Co. Ltd. China) with a constant voltage of 40 V at room temperature for 1 h. The as-prepared TiO_2NTWs were thoroughly washed with ethanol and then DI water, and then annealed in the air at 450 °C for 2 h.

2.2 Hydrogen treatment

The pristine TiO_2NTWs were annealed in hydrogen atmosphere at different temperatures in a range of 250–550 °C. The preparation was performed in a home-built tube furnace filled with ultrahigh purity hydrogen gas (Praxair).

2.3 Preparation of quantum dots sensitized H*TiO_2NTWs

Quantum dots were assembled onto TiO_2NTWs by SILAR technique. For CdS modification, the H*TiO_2NTWs was successively immersed into two different solutions for 10 min each, first in 0.50 M $Cd(NO_3)_2 \cdot 4H_2O$ in ethanol and then in 0.50 M Na_2S in deionized water. Following each immersion, the films were respectively rinsed with pure ethanol and deionized water to remove excess precursors and dried in air before the next dipping. This is called one SILAR cycle.

Similarly, for PbS sensitization, the sample was dipped into the 0.02 M $Pb(NO_3)_2$ solution (obtained by dissolving $Pb(NO_3)_2$ in methanol/water with volume ratios of 1 : 1) for 5 min then dipped into 0.02 M Na_2S methanol solution for 5 min.

For the hybrid CdS/PbS co-sensitized samples, the PbS deposition was carried out immediately after CdS deposition. Then 3 cycles of ZnS layers were then deposited to protect the PbS QDs from chemical corrosion and to suppress back-reaction of the photo-injected electrons. Eventually, the samples were annealed at 300 °C for 1 h in nitrogen.

2.4 Characterization

Scanning electron microscopy (SEM) images were collected with a field-emission SEM (JEOL JSM-6700F). Transmission electron microscope (TEM) and high-resolution TEM (HR-TEM) images were obtained with a JEM-2100F high-resolution transmission microscope operating at 200 kV. Scanning TEM and energy-dispersive X-ray spectroscopy analyses (STEM-EDX) were taken by a FEI TECNAI F20 transmission electron microscope with an accelerating voltage of 200 kV. X-ray diffraction (XRD) spectra of samples were collected with a Rigaku D/max-ray diffractometer with Cu Kα radiation ($\lambda = 1.5418$ Å). Optical characterization of the films was performed using a UV-3150 double-beam spectrophotometer.

2.5 Photoelectrochemical measurements

All photoelectrochemical properties measurements were performed in a three-electrode electrochemical system, which is made of quartz cell and linked with the electrochemical workstation (CH Instruments, model CHI601C), using a Ag/AgCl reference electrode and a Pt wire as the counter electrode. The samples were fabricated into photoanodes with a well-defined area of 1 cm^2. Linear sweeps were collected in a mixture of 0.25 M $Na_2S \cdot 9H_2O$, 0.35 M Na_2SO_3 and 0.1 M KCl aqueous solution, under simulated sunlight illumination at 100 mW cm^{-2} from a 500 W xenon lamp (Spectra Physics). The CHI electrochemical workstation was used to measure dark and illuminated current at a scan rate of 10 mV s^{-1}. The light intensity was calibrated by using a laser powermeter (BG26M92C, Midwest Group), equivalent to AM 1.5 G light at 100 mW cm^{-2}.

3. Results and discussion

3.1 Sample characterization

The SEM images of the pristine TiO_2NTWs, the H*TiO_2NTWs, the H*TiO_2NTWs/CdS and the H*TiO_2NTWs/CdS/PbS are shown in Fig. 1. Fig. 1A shows the top view of the pristine TiO_2NTWs morphology, loosely arranged nanowires are on the top of the nanotubes and some pores are exposed. As anodization allows for the preparation of TiO_2 nanotubes, TiO_2 nanowires was formed on the TiO_2 nanotubes with the effect of electric-field-directed chemical etching.[5] Fig. 1B is the cross-section view of the TiO_2NTWs, with a smooth nanotube length of about 2.8–3 μm and an average pore diameter of 90 nm. The inset in Fig. 1B is the cross-section view of H*TiO_2NTWs which is obviously that after hydrogen treatment the tubes are still smooth. Fig. 1C and D show the top and cross-section view of H*TiO_2NTWs coated by CdS QDs after 4 SILAR cycles, respectively. After assembled with CdS, the nanotubes and nanowires become rougher which are observed as shown in Fig. 1D. After deposition of PbS for 3 cycles, the surfaces of H*TiO_2NTWs/CdS NTWs become much rougher as shown in Fig. 1E and F, which reveals that QDs have covered almost the entire surfaces of TiO_2NTWs.

The detailed microscopic characterization of H*TiO_2NTWs array deposited with CdS/PbS/ZnS for 4 cycles/2 cycles/3 cycles were performed by using TEM and high-resolution TEM (HR-TEM). Fig. 2A shows the TEM image of H*TiO_2 NTWs, it can be seen that nanowires are formed on the top of nanotubes, Fig. 2B shows the TEM image of bare H*TiO_2 nanotube, the tube is relatively smooth. Fig. 2C provides the TEM image of the sample which we can see that the whole surface area of TiO_2NTWs is covered with QDs that have size smaller than 10 nm. The HR-TEM image of H*TiO_2NTWs/CdS/PbS/ZnS is shown in Fig. 2D, the heterojunction region have indicated the high crystallinity of TiO_2NTWs, CdS, PbS, and ZnS. The lattice fringes with interplanar spacing (lattice distance) $d_{\{101\}} = 0.351$ nm in Fig. 2B is consistent with the antase phase of TiO_2 [JCPDS no. 71-1166]. As is shown in the graph, around the TiO_2 crystallite, fine crystallites with various orientations and lattice spacing are found. By carefully measured and compared with the lattice

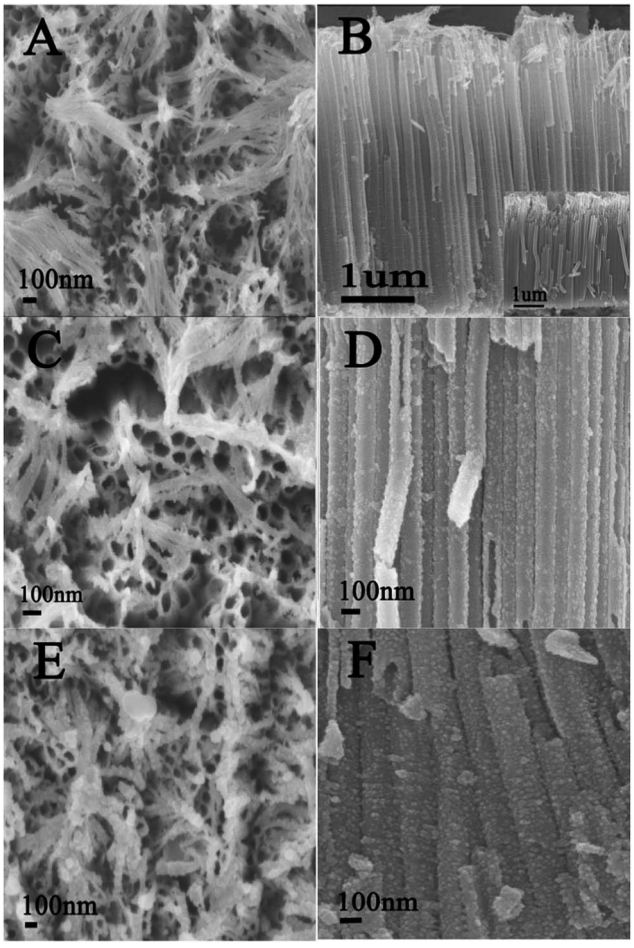

Fig. 1 Field-emission scanning electron microscopy (FESEM) images: (A) and (B) are top view and cross-section view of bare TiO_2NTWs, respectively; the inset in (B) represents a cross-section view of H*TiO_2NTWs (pristine TiO_2NTWs after hydrogen treatment); (C) and (D) are top view and cross-section view of H*TiO_2NTWs/CdS (4 cycles) electrode, respectively; (E) and (F) are cross-section views of H*TiO_2NTWs/CdS (4 cycles)/PbS (2 cycles), respectively. For the sake of a better investigation on the growth of CdS and PbS, so the samples prepared for FESEM did not cap ZnS.

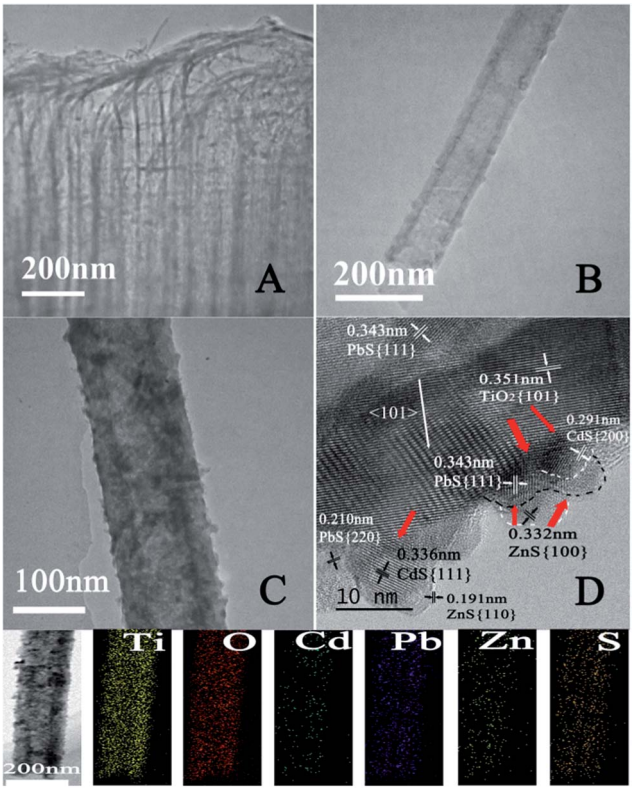

Fig. 2 (A) TEM image of H*TiO_2 nanotubes with nanowires on top; (B) TEM image of bare H*TiO_2 nanotube; (C) TEM image of H*TiO_2NTWs/CdS/PbS/ZnS electrode; (D) HR-TEM images of H*TiO_2NTWs/CdS/PbS/ZnS electrode; STEM images and corresponding STEM-EDX elemental mapping of the sample (H*TiO_2NTWs/CdS(4 cycles)/PbS(2 cycles)/ZnS(3 cycles))are shown, revealing the homogeneous distribution of Cd, S, Pb and Zn elements over the whole TiO_2NTWs.

parameters date of JCPDS, the crystallites connecting to TiO_2-NTWs have lattice distances of $d_{\{111\}} = 0.336$ nm, $d_{\{200\}} = 0.291$ nm, which are correspond to the cubic phase of CdS [JCPDS no. 80-0019]. The outer layer crystallites next to the CdS layer and lattices of Fig. 2B have lattice fringes of $d_{\{111\}} = 0.343$ nm and $d_{\{220\}} = 0.210$ nm are correspond to the cubic phase of PbS [JCPDS no. 77-0244]. In Fig. 2B, we can also see that the {100} and {110} planes of the wurtzite phase of ZnS [JCPDS no. 75-1547] are stacked outside the PbS and CdS with different angles. Moreover, refer to the area where red arrows exist in Fig. 2B, there are four dominant interfaces of TiO_2NTWs/CdS, TiO_2-NTWs/PbS, TiO_2NTWs/CdS/PbS and TiO_2NTWs/CdS/PbS/ZnS. It is clearly that the {200} planes of CdS and the {111} planes of PbS are connected to the {101} planes of TiO_2NTWs with certain angles, which means the CdS and PbS are grown on the TiO_2-NTWs. These results demonstrate that CdS, PbS and ZnS QDs have been successfully deposited on the surface of TiO_2NTWs to form a TiO_2NTWs/CdS/PbS cascading band structure. STEM images and corresponding STEM-EDX elemental mapping of the sample (H*TiO_2NTWs/CdS/PbS/ZnS) was also shown to reveal the distribution of Cd, Pb, Zn and S elements over the whole TiO_2NTWs. This also prove that hydrogen treatment do not introduce any impurities. XRD spectra of the pristine TiO_2NTWs and H*TiO_2NTWs prepared at various annealing temperatures from 250 °C to 500 °C were collected to determine the crystal structure and possible phase changes during hydrogen annealing (Fig. 3A). The pristine TiO_2NTWs were crystallized in anatase phases [JCPDS no. 71-1166]. And the diffraction strongest peak centered at 2-theta of 25.4° corresponds to the crystal face {101} which is providing evidence that the TiO_2NTWs are highly oriented in the ⟨101⟩ direction on the Ti foil. It can be seen that there is no phase change after hydrogen treatment (250 °C to 400 °C), and hydrogen was chosen not only because it is a reducing gas with very light weight that may facilitate diffusion of the gas into TiO_2, but ultra-high-purity hydrogen can also avoid the possibility of introducing of impurities. And at the temperature of 450 °C and 500 °C, there comes a new peak corresponds to rutile TiO_2 [JCPDS no. 86-0147]. Fig. 3B shows the XRD patterns of pristine TiO_2NTWs (a), H*TiO_2NTWs (b), H*TiO_2NTWs/CdS (c), H*TiO_2NTWs/CdS/PbS (d) and H*TiO_2/CdS/PbS/ZnS (e) electrode. No fresh evident diffraction peaks are observed for the little amount of CdS/ZnS QDs and their highly dispersion on TiO_2NTWs surface. After sensitization of PbS nanocrystals, TiO_2NTWs exhibit a new small peak at 2-theta of 30.2°, this new peak can be indexed to the {200} planes of the cubic-phase PbS [JCPDS no. 77-0244], which correspond well to the results we got from Fig. 2B. Meanwhile, we performed energy dispersive X-ray spectroscopy (EDX) analysis to determine the existence of CdS, PbS and ZnS in H*TiO_2NTWs/CdS/PbS/ZnS (Fig. 3C). And Cd, Pb, Zn and S elements are found and no impurities to be present.

Fig. 4 shows the UV-vis absorption spectra of pristine TiO_2NTWs,H*TiO_2NTWs,H*TiO_2NTWs/CdS(4c),H*TiO_2NTWs/CdS(4c)/PbS(2c) and H*TiO_2NTWs/CdS(4c)/PbS(2c)/ZnS(3c) electrodes. It is obviously that pristine TiO_2NTWs (Fig. 4a) absorb mainly UV light with a wavelength around 370 nm, and

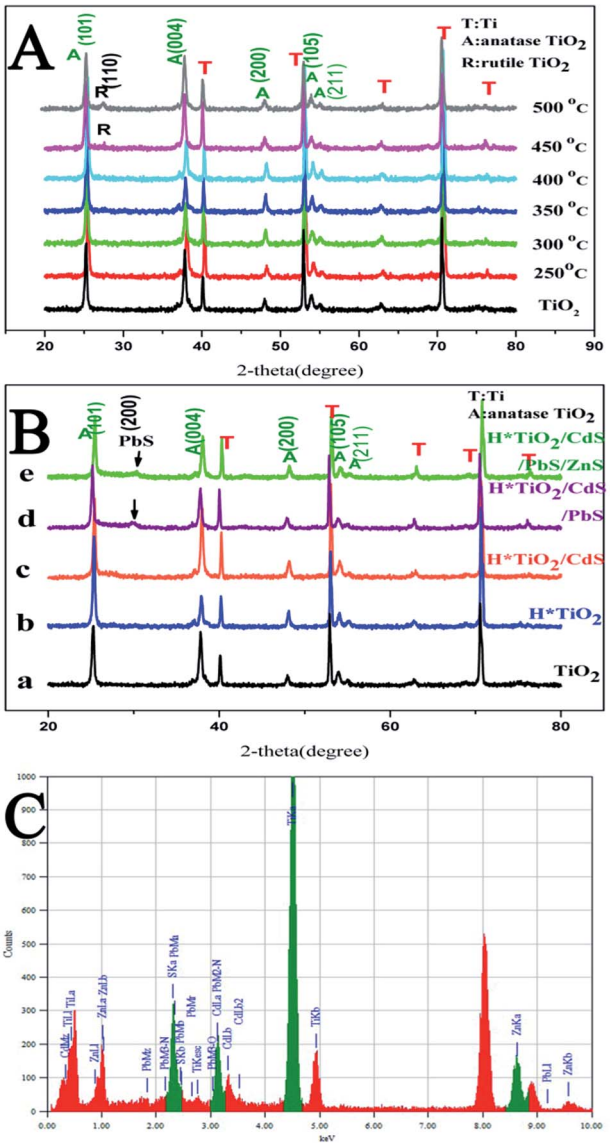

Fig. 3 (A) XRD patterns of pristine TiO_2 NTWs and H*TiO_2 NTWs annealed in hydrogen at various temperatures (from 250 to 500 °C); (B) XRD patterns of (a) pristine TiO_2NTWs (b) H*TiO_2NTWs (c) H*TiO_2/CdS (d) H*TiO_2/CdS/PbS (e) H*TiO_2/CdS/PbS/ZnS electrode; (C) EDX spectrum of H*TiO_2/CdS/PbS/ZnS electrode.

no significant absorbance can be seen in the visible region. However, the absorption edge of H*TiO_2NTWs (Fig. 4b) is about 380 nm which shows a tiny red-shift in the absorption than pristine TiO_2NTWs, in the meantime, the absorbance in all region of H*TiO_2NTWs is a little stronger than that of TiO_2-NTWs, indicating that hydrogen treatment has improved the absorption property of the TiO_2NTWs by narrowing the corresponding band gap *via* changing the surface bonding as well as the electronic valence band position of TiO_2NTWs.[35,36] With the deposition of CdS on TiO_2NTWs, the absorption spectra of the CdS-sensitized NTWs (Fig. 4c) extend into the visible region and the absorption edge of the CdS-sensitized NTWs is nearly 555 nm. Still, the UV-vis spectra of H*TiO_2NTWs/CdS/PbS (Fig. 4d) shows a strong absorption in the visible region, indicating that

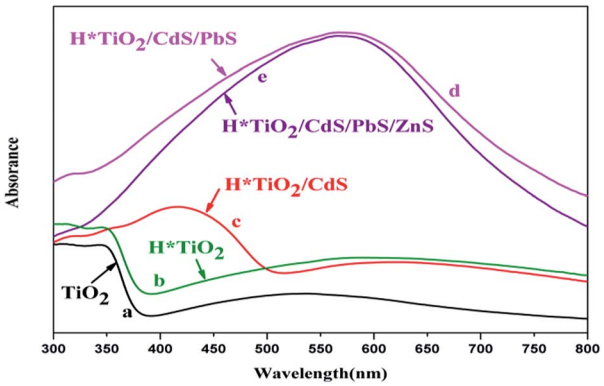

Fig. 4 UV-vis absorption spectra of (a) pristine TiO_2NTWs (b) H*TiO_2NTWs (c) H*TiO_2/CdS (d) H*TiO_2/CdS/PbS (e) H*TiO_2/CdS/PbS/ZnS electrode.

the co-modification effect of H-SILAR can significantly extend the absorption range and increase the absorption property of the TiO_2 NTWs. A blue shift occurs after ZnS QDs decoration of H*TiO_2/CdS/PbS (Fig. 4e), indicating that the absorption ability is slightly weakened by ZnS QDs on the exterior of PbS with wider band gaps.

3.2 Photoelectrochemical performance of the electrodes

The photoelectrochemical performances of these samples in the dark and with one sun (100 mW cm^{-2}) illumination were shown in Fig. 5. The observed dark current densities for all electrodes are negligible. The effect of hydrogen treatment and multiple semiconductors co-sensitization (H-SILAR) of the device performance had been carefully studied here and found the electrode prepared by annealing in hydrogen at 350 °C for 30 min and using 4 cycles of CdS plus 2 cycles of PbS with 3 cycles ZnS exhibits the best performance.

Fig. 5A shows the *J–V* curves of TiO_2NTWs annealing in hydrogen at various temperatures in a range of 250–500 °C for 30 min. It's clearly that the photocurrent density of H*TiO_2-NTWs increase gradually with the increase of the hydrogen annealing temperature from 250 to 350 °C. The H*TiO_2NTWs annealed at 350 °C for 30 min has best performance with maximum photocurrent density of 0.90 mA cm^{-2}, which is almost twice what we got from pristine TiO_2NTWs. The color of the TiO_2NTWs depends on the hydrogen annealing temperature. With the increase of annealing temperature, the color of TiO_2NTWs become darker (the inset of Fig. 5A). The black color maybe ascribed to surface oxygen vacancies of TiO_2NTWs. We deduce from Fig. 5A that with the increase of annealing temperature, the oxygen vacancies increase simultaneously. Oxygen vacancies act as donor density and contribute improving the photoactivity of TiO_2NTWs.[37] However, too much oxygen vacancies may result in the recombination of the charge, which is the reason why photocurrent density reduces with the hydrogen annealing temperature over 350 °C. As seen in Fig. 5B, the optimal cycle found for the CdS-sensitized H*TiO_2NTWs electrodes is about 4 cycles with 2.71 mA cm^{-2}. As seen the comparison of (i) and

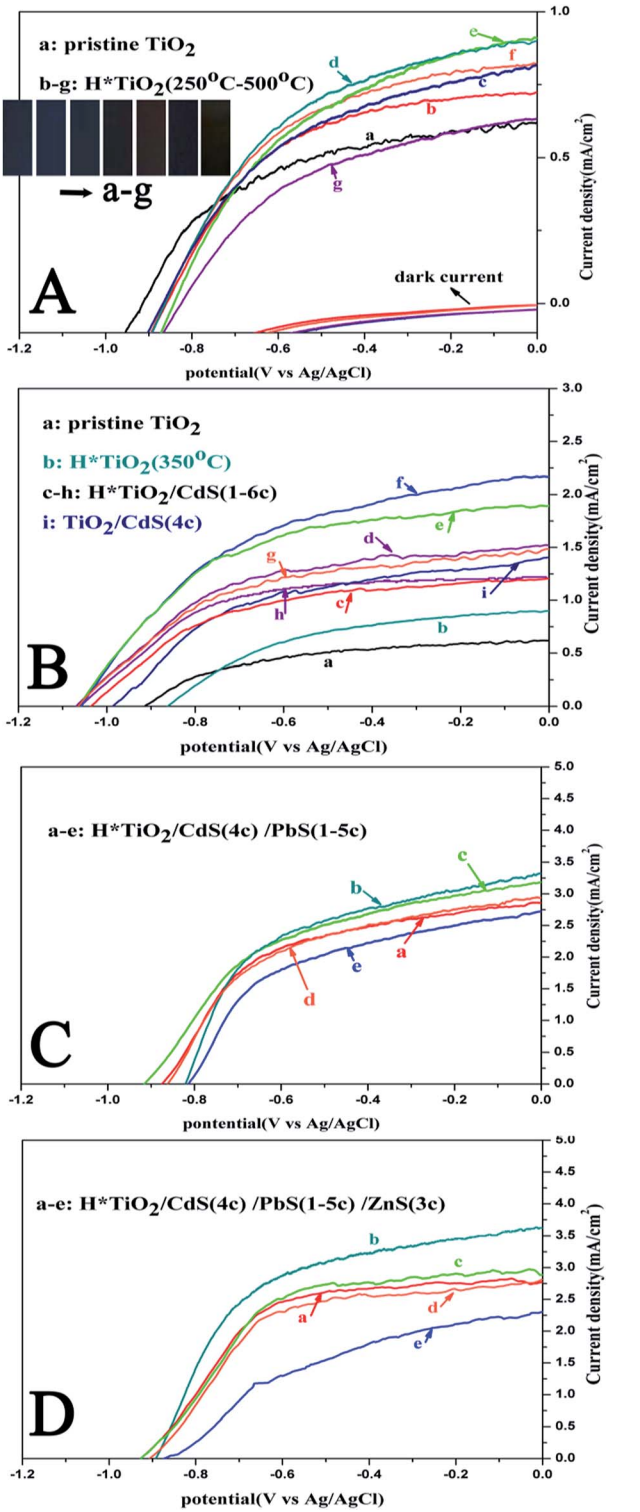

Fig. 5 (A) Photocurrent–voltage (*J–V*) curves of pristine TiO_2NTWs(a), H*TiO_2NTWs at different temperature from 250 to 500 °C (b)–(g), the inset in (A) were digital pictures of (a)–(g); (B) TiO_2NTWs (a), H*TiO_2(350 °C) (b), H*TiO_2(350 °C) with 1–6 cycles of CdS(c)–(h), pristine TiO_2 with 4 cycles of CdS(i); (C) H*TiO_2 (350 °C)/CdS (4 cycles) with 1–5 cycles of PbS (a)–(e); (D) H*TiO_2 (350 °C)/CdS (4 cycles) with 1–5 cycles of PbS and 3 cycles of ZnS (a)–(e).

(f) in Fig. 5B, we find that H*TiO_2/CdS (4c) presents a much better performance than pristine TiO_2/CdS (4c). We kept CdS at 4 cycles when we fabricated H*TiO_2NTWs/CdS/PbS/ZnS (3c) photoelectrodes and the corresponding *J–V* curves are shown in Fig. 5D. The maximum photocurrent density of 3.62 mA cm^{-2} is attained, which can boost the photocurrent density of the pristine TiO_2NTWs by up to 503%. The cascade energy level structure (Scheme 1) in the order of TiO_2NTWs < CdS < PbS is formed *via* the combination of CdS and PbS, as reported by others.[38] The favorable alignment of the fermi levels at TiO_2NTWs/CdS/PbS interfaces facilitates electron injection and hole recovery for both inner CdS and outer PbS layers. In the meantime, the CdS layer promotes the growth of the PbS layer due to less mismatched constants and more similar chemistries between them. Coating the PbS with ZnS layer is a approach that other researchers have found to be useful in maintaining the photo-stability of photoelectrodes.[39] As a wide band gap semiconductor, ZnS has been extensively deposited on QDs on the surface of photoanodes to suppress electron leakage from QDs to the electrolyte.[40,41] Hao Wang *et al.* have indicated that for ZnO/CdTe nanocable arrays photoanode, ZnS not only serves as a barrier layer that prevents electron injection from CdTe to the electrolyte but also provides an effective tunneling channel for hole transfers to the electrolyte.[42] As seen in Fig. 5C, the photoelectrochemical performances of H*TiO_2 (350 °C)/CdS (4 cycles) with 1–5 cycles of PbS were investigated. The maximum photocurrent density of 3.33 mA cm^{-2} is obtained (H*TiO_2 (350 °C)/CdS (4 cycles)/PbS(2 cycles)), which is slightly lower than 3.62 mA/cm^2 (H*TiO_2 (350 °C)/CdS (4 cycles)/PbS (2 cycles)/ZnS (3 cycles)). Although a blue shift occurs after ZnS QDs decoration of H*TiO_2/CdS/PbS (Fig. 4), the photo-electrochemical performances of H*TiO_2/CdS/PbS/ZnS is still relatively better than H*TiO_2/CdS/PbS, this phenomenon maybe caused by the existence of ZnS and ZnS serves as a barrier layer for electron injections from the absorbing layer to the electrolyte (Scheme 1C). Furthermore, Hodes[43] suggested that even if the valence band edge of ZnS is below that of PbS, hole transfer may still be possible if the ZnS layer is adequately thin such that hole tunneling or hole transfer through surface states in the ZnS layer is allowed. The ZnS layer over PbS in the H*TiO_2/CdS/PbS/ZnS is discontinuous (Fig. 2D), with sizes about 5 nm, and smaller ZnS nanocrystals may provide effective pathways for hole tunneling to the electrolyte. This result shows that visible-light-induced photoelectrochemical performances of the pristine TiO_2NTWs were significantly improved by the H-SILAR approach.

This tubular and crystal structure of TiO_2NTWs has the advantage of the tube, such as efficient charge separation and transport properties as well as superior light harvesting efficiency while the wires that exposed in the electrolyte and favor more nanoparticles growth. It also should be noted that electron transfer occurs only when both semiconductors in heterojunction are in close contact, which contributed to the increasing photocurrent density. And Fig. 2B is a stronger confirmation as the QDs are successful grown on TiO_2. More importantly, the increase oxygen vacancies would help the adsorption of Cd^{2+} and Pb^{2+} on the surface of TiO_2 during SILAR, and thus increase the formation of heterojunction. As analyzed from SEM and TEM (Fig. 1 and 2), PbS and CdS QDs co-sensitized TiO_2 prepared through H-SILAR approach led to a uniform and intimate coating of QDs inside NTs. This structure can not only efficiently increase the path length of light in the QDs layer but also facilitate charge separation. Compared with pristine TiO_2NTWs electrode, as shown in Fig. 4, the H*TiO_2/CdS/PbS/ZnS electrode has a super stronger absorption in the visible region, which greatly raised the utilization rate of the solar energy. These factors jointly contribute to the enhancement of photoelectrochemical performances of our sample.

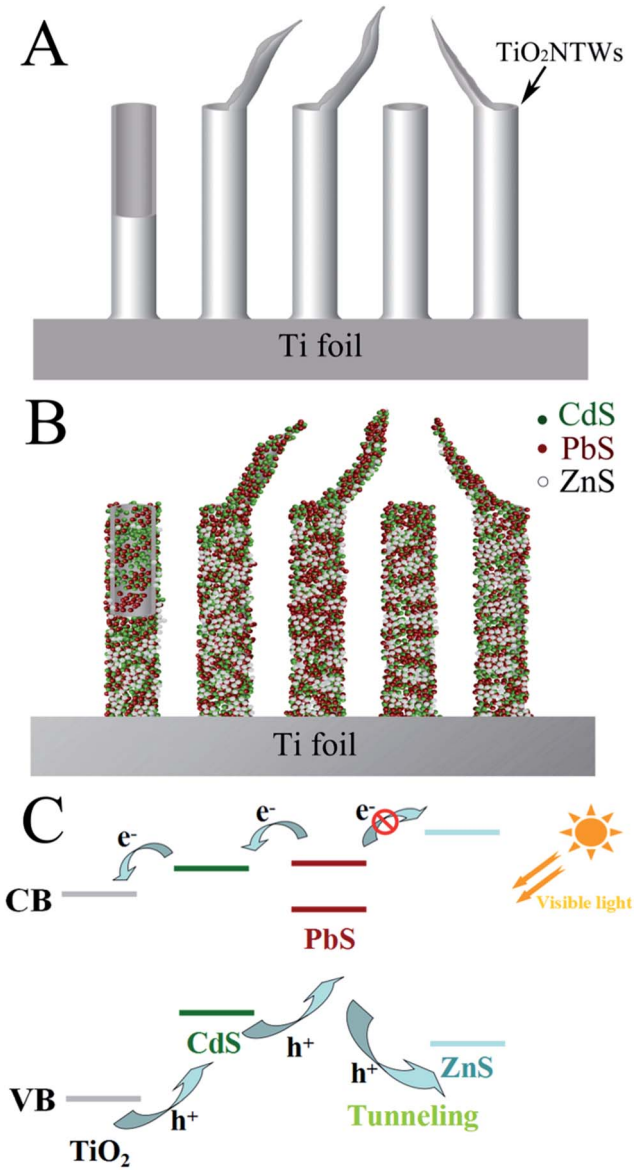

Scheme 1 (A) Schematic diagram of the nanostructure of pristine TiO_2NTWs; (B) CdS, PbS and ZnS QDs modified TiO_2NTWs electrode; (C) charge-transfer processes among PbS, CdS, ZnS and TiO_2.

4. Conclusions

In summary, our work has demonstrated that H-SILAR can be used as an easy and general approach to fundamentally improve the photoelectrochemical activity of TiO_2 photoelectrodes. The best performance of photoelectrode was co-sensitized 4 cycles of CdS plus 2 cycles of PbS with 3 cycles ZnS on TiO_2 NTWs treated in hydrogen at 350 °C. This modified photoelectrode shows significant enhancement in the photoelectrochemical activity compared with pristine TiO_2 NTWs. As shown in Fig. 1, 2, the NTWs array structure provides a direct electron pathway to the Ti substrate over a large surface area and contributes significantly to formation of QDs-TiO_2 heterojunction architecture. UV-vis absorption spectra analyses confirm that the photocurrent enhancement is mainly due to the greatly improved photoactivity in the UV and visible region. Two reasons lead to this significant improvement of photoactivity. One is increased donor density caused by the formation of oxygen vacancies in H*TiO_2 samples. The other is the cascade energy level structure creates an efficient charge-carrier transfer channel and would trigger a high resistance to transport of excited electrons (Scheme 1C). In our experiment, the photoelectrode results in a large photogenerated photocurrent of 3.62 mA cm^{-2} under visible light illumination of AM 1.5 G, which can boost the photocurrent density of the pristine TiO_2NTWs by up to 503%. More importantly, it opens up new opportunities in various areas such as PEC water splitting, recycled photocatalyst and solar cells.

Acknowledgements

This work was financially supported by the Science and Technology Development Program of Jilin Province (no. 20110417) and the National Natural Science Foundation of China (no. 51272086).

Notes and references

1 N. Zhang, Y. Zhang and Y. J. Xu, Recent progress on graphene-based photocatalysts: current status and future perspectives, *Nanoscale*, 2012, **4**, 5792.
2 K. Shankar, J. I. Basham, N. K. Allam, O. K. Varghese, G. K. Mor, X. Feng, M. Paulose, J. A. Seabold, K. S. Choi and C. A. Grimes, Recent Advances in the Use of TiO_2 Nanotube and Nanowire Arrays for Oxidative Photoelectrochemistry, *J. Phys. Chem. C*, 2009, **113**, 6327.
3 B. Tan and Y. Wu, Dye-Sensitized Solar Cells Based on Anatase TiO_2 Nanoparticle-Nanowire Composites, *J. Phys. Chem. B*, 2006, **110**, 15932.
4 X. Chen and S. S. Mao, Titanium Dioxide Nanomaterials: Synthesis, Properties, Modifications, and Applications, *Chem. Rev.*, 2007, **107**, 2891.
5 J. H. Lim and J. Choi, Titanium Oxide Nanowires Originating from Anodically Grown Nanotubes: The Bamboo-Splitting Model, *Small*, 2007, **3**, 1504.
6 H. A. Hamedani and S. W. Lee, Synthesis and Growth Mechanism of Thin-Film TiO_2 Nanotube Arrays on Focused-Ion-Beam Micropatterned 3D Isolated Regions of Titanium on Silicon, *ACS Appl. Mater. Interfaces*, 2013, **5**, 9026.
7 M. Y. Zhang, C. L. Shao, J. B. Mu, Z. Y. Zhang, Z. C. Guo, P. Zhang and Y. C. Liu, One-dimensional Bi_2MoO_6/TiO_2 hierarchical heterostructures with enhanced photocatalytic activity, *CrystEngComm*, 2012, **14**, 605.
8 A. Fujishima and K. Honda, Electrochemical Photolysis of Water at a Semiconductor Electrode, *Nature*, 1972, **238**, 37.
9 M. Grätzel, Photoelectrochemical Cells, *Nature*, 2001, **414**, 338.
10 X. L. Cui, M. Ma, W. Zhang, Y. H. Yang and Z. J. Zhang, Nitrogen-doped TiO_2 from TiN and its visible light photoelectrochemical properties, *Electrochem. Commun.*, 2008, **10**, 367.
11 A. B. Murphy, Does carbon doping of TiO_2 allow water splitting in visible light? Comments on "Nanotube enhanced photoresponse of carbon modified (CM)-n-TiO_2 for efficient water splitting", *Sol. Energy Mater. Sol. Cells*, 2008, **92**, 363.
12 R. Ashai, T. Morokawa, T. Ohwaki and Y. Taga, Visible-Light Photocatalysis in Nitrogen-Doped Titanium Oxides, *Science*, 2001, **293**, 269.
13 G. Wang, H. Wang, Y. Ling, Y. Tang, X. Yang, R. C. Fitzmorris, C. Wang, J. Z. Zhang and Y. Li, Hydrogen-Treated TiO_2 Nanowire Arrays for Photoelectrochemical Water Splitting, *Nano Lett.*, 2011, **11**, 3026.
14 R. Sanjinès, H. Tang and H. Berger, *et al.* Electronic structure of anatase TiO_2 oxide, *J. Appl. Phys.*, 1994, **75**, 2945.
15 Q. H. Li, L. Wei, Y. R. Xie and F. Jiang, *et al.* Effects of oxygen vacancy on the electrical and magnetic properties of anatase $Fe_{0.05}Ti_{0.95}O_{2-\delta}$ films, *J. Alloys Compd.*, 2013, **574**, 67.
16 H. Tang, K. Prasad and R. Sanjinèsetal, *et al.* Electrical and optical properties of TiO_2 anatae thin films, *J. Appl. Phys.*, 1994, **75**, 2042.
17 X. Chen, L. Liu, P. Y. Yu and S. S. Mao, Ti^{3+}in the Surface of Titanium Dioxide: Generation, Properties and Photocatalytic Application, *Science*, 2011, **331**, 746.
18 S. Hoang, S. P. Berglund, N. T. Hahn, A. J. Bard and C. B. Mullins, Enhancing Visible Light Photo-oxidation of Water with TiO_2 Nanowire Arrays via Cotreatment with H_2 and NH_3: Synergistic Effects between Ti^{3+} and N, *J. Am. Chem. Soc.*, 2012, **134**, 3659.
19 I. Nakamura, N. Negishi and S. Kutsuna, *et al.* Role of oxygen vacancy in the plasma-treated TiO_2 photocatalyst with visible light activity for NO removal, *J. Mol. Catal. A: Chem.*, 2000, **161**, 205.
20 M. K. Nowotny, L. R. Sheppard, T. Bak and J. Nowotny, Defect Chemistry of Titanium Dioxide. Application of Defect Engineering in Processing of TiO_2-Based Photocatalysts, *J. Phys. Chem. C*, 2008, **112**, 5275.
21 F. Fabregat-Santiago, E. M. Barea, J. Bisquert, G. K. Mor, K. Shankar and C. A. Grimes, High Carrier Density and Capacitance in TiO_2 Nanotube Arrays Induced by Electrochemical Doping, *J. Am. Chem. Soc.*, 2008, **130**, 11312.
22 A. Janotti, J. B. Varley, P. Rinke, N. Umezawa, G. Kresse and C. G. Van de Walle, Hybrid functional studies of the oxygen

vacancy in TiO_2, *Phys. Rev. B: Condens. Matter Mater. Phys.*, 2010, **81**, 085212.

23 M. S. Park, S. K. Kwon and B. I. Min, Electronic structures of doped anatase TiO_2: $Ti_{1-x}M_xO_2$ (M = Co, Mn, Fe, Ni), *Phys. Rev. B: Condens. Matter Mater. Phys.*, 2002, **65**, 1612012.

24 C. H. Chang and Y. L. Lee, Chemical bath deposition of CdS quantum dots onto mesoscopic TiO_2 films for application in quantum-dot-sensitized solar cells, *Appl. Phys. Lett.*, 2007, **91**, 053503.

25 H. I. Okur, Y. Türker and O. Dag, Synthesis of Stable Mesostructured Coupled Semiconductor Thin Films: meso-CdS-TiO_2 and meso-CdSe-TiO_2, *Langmuir*, 2010, **26**, 538.

26 L. P. Wu, Y. L. Zhang, L. Z. Long, C. P. Cen and X. J. Li, Effect of ZnS buffer layers in ZnO/ZnS/CdS nanorod array photoelectrode on the photoelectrochemical performance, *RSC Adv.*, 2014, **4**, 20716.

27 L. Wu, J. Li, S. Zhang, L. Long, X. Li and C. Cen, Effect of Ordered TiO_2 Nanotube Array Substrate on Photocatalytic Performance of CdS-Sensitized ZnO Nanorod Arrays, *J. Phys. Chem. C*, 2013, **117**, 22591.

28 Q. Shen, D. Arae and T. Toyoda, Photosensitization of nanostructured TiO_2 with CdSe quantum dots: effects of microstructure and electron transport in TiO_2 substrates, *J. Photochem. Photobiol., A*, 2004, **164**, 75.

29 W. Guo, Y. Shen, M. Wu, L. Wang, L. Wang and T. Ma, SnS-Quantum Dot Solar Cells Using Novel TiC Counter Electrode and Organic Redox Couples, *Chem.–Eur. J.*, 2012, **18**, 7862.

30 P. Hoyer and R. Könenkamp, Photoconduction in Porous TiO_2 Sensitized by PbS Quantum Dots, *Appl. Phys. Lett.*, 1995, **66**, 349.

31 Y. Li, L. Wei, X. Chen, R. Zhang, X. Sui, Y. Chen, J. Jiao and L. Mei, Efficient PbS/CdS co-sensitized solar cells based on TiO_2 nanorod arrays, *Nanoscale Res. Lett.*, 2013, **8**, 67.

32 Z. Q. Lin, Y. K. Lai, R. G. Hu, J. Li, R. G. Du and C. J. Lin, A highly efficient ZnS/CdS@TiO_2 photoelectrode for photogenerated cathodic protection of metals, *Electrochim. Acta*, 2010, **55**, 8717.

33 H. J. Lee, J. Bang, J. Park, S. Kim and S. M. Park, Multilayered Semiconductor (CdS/CdSe/ZnS)-Sensitized TiO_2 Mesoporous Solar Cells: All Prepared by Successive Ionic Layer Adsorption and Reaction Processes, *Chem. Mater.*, 2010, **22**, 5636.

34 J. Jiao, Z. J. Zhou, W. H. Zhou and S. X. Wu, CdS and PbS quantum dots co-sensitized TiO_2 nanorod arrays with improved performance for solar cells application, *Mater. Sci. Semicond. Process.*, 2013, **16**, 435.

35 Z. Zheng, B. Huang and J. Lu, *et al.* Hydrogenated titania: synergy of surface modification and morphology improvement for enhanced photocatalytic activity, *Chem. Commun.*, 2012, **48**, 5733.

36 X. Pan, M. Q. Yang, X. Fu, N. Zhang and Y. J. Xu, Defective TiO_2 with oxygen vacancies: synthesis, properties and photocatalytic applications, *Nanoscale*, 2013, **5**, 3601.

37 X. B. Chen, L. Liu, Z. Liu, M. A. Marcus, W. C. Wang, N. A. Oyler, M. E. Grass, B. H. Mao, P. A. Glans, P. Y. Yu, J. H. Gao and S. S. Mao, Properties of disorder-engineered black titanium dioxide nanoparticles through hydrogenation, *Sci. Rep.*, 2013, **3**, 1510.

38 M. A. Hossain, Y. K. Zhen and Q. Wang, PbS/CdS-sensitized mesoscopic SnO_2 solar cells for enhanced infrared light harnessing, *Phys. Chem. Chem. Phys.*, 2012, **14**, 7367.

39 Q. Shen, J. Kobayashi, L. J. Diguna and T. Toyoda, Effect of ZnS coating on the photovoltaic properties of CdSe quantum dot-sensitized solar cells, *J. Appl. Phys.*, 2008, **103**, 084304.

40 S. H. Kim, D. Fan, J. J. Kim, D. W. Jung, S. O. Kang and J. Ko, Highly efficient CdSe quantum-dot-sensitized TiO_2 photoelectrodes for solar cell applications, *Electrochem. Commun.*, 2009, **11**, 1337.

41 A. Salant, M. Shalom, I. Hod, A. Faust, A. Zaban and U. Banin, Quantum Dot Sensitized Solar Cells with Improved Efficiency Prepared Using Electrophoretic Deposition, *ACS Nano*, 2010, **4**, 5962–5968.

42 X. Wang, R. Liu, T. Wang, B. Wang, Y. Xu and H. Wang, Dual Roles of ZnS Thin Layers in Significant Photocurrent Enhancement of ZnO/CdTe Nanocable Arrays Photoanode, *ACS Appl. Mater. Interfaces*, 2013, **5**, 3312.

43 H. M. Chen, K. C. Chen, Y. C. Chang, C. W. Tsai, R. S. Liu, S. F. Hu, W. S. Chang and K. H. Chen, Quantum Dot Monolayer Sensitized ZnO Nanowire-Array Photoelectrodes: True Efficiency for Water Splitting, *Angew. Chem., Int. Ed.*, 2010, **49**, 5966–5969.